Study of Nuclear States in ^{40}Ca by Inelastic Electron Scattering

K. Itoh, M. Oyamada, and Y. Torizuka

Laboratory of Nuclear Science, Tohoku University, Sendai, Japan

(Received 16 July 1970)

High-resolution measurements of the differential cross sections for inelastic electron scattering of 183- and 250-MeV electrons by ^{40}Ca were carried out using beams from the Tohoku 300-MeV electron linear accelerator. Peaks were found with the following excitation energies (in MeV), and spins and parities: $3.74(3^-)$, $3.90(2^+)$, $4.49(5^-)$, $5.25(2^+)$, $5.61(2^+)$, $5.90(1^-)$, $6.29(3^-)$, $6.59(3^-)$, $6.95(1^-)$, $7.9(2^+,4^+)$, $8.5(2^+,4^+,5^-)$, and others in the giant-resonance region. The cross sections for these states were obtained in the momentum transfer range from 0.5 to 2.2 F^{-1}. The data of the 3^- and 5^- states were compared not only with Tassie's vibrational model, but also with the particle-hole model of Gillet *et al*. The excitations of the dipole states $(T=0)$ are compared with Fujii's calculation. The data have been analyzed by using a distorted-wave code of Tuan, Wright, and Onley to extract the values of the reduced transition probabilities using the transition charge desities ρ_{tr} modified from the Tassie model, and from the particle-hole model. Then, the values of $B(EL)$ obtained from the quite different models are compared. The shapes of ρ_{tr} which provide best fits to the data are presented.

I. INTRODUCTION

Inelastic electron scattering from nuclei using deeply penetrating high-energy electrons are particularly valuable as a means of investigating the nuclear structure.[1,2] Since the basic interaction between the projectile and the target is well known, one can immediately relate the cross section of the electroexcitation to the reduced matrix element of the charge and current density operators taken between the initial and final nuclear states. Then, the wave functions for these states, which are calculated by assuming a nuclear model, determine the behavior of the cross section as a function of momentum transfer, which shows, in general, diffraction structure as momentum transfer is increased. Thus, electron scattering from a nucleus, such as ^{40}Ca, carried out at momentum transfers higher than 1 F^{-1} may be a crucial test of the nuclear models employed. Some experiments of this type have been carried out on the ^{40}Ca nucleus.[3,4] However, information from previous experiments has been limited by a lack of energy resolution of the measurements.

We have carried out high-resolution measurements of the differential cross sections for inelastic scattering of 183- and 250-MeV electrons from the ^{40}Ca nucleus. The cross sections for excitations up to 9 MeV were obtained in the momentum transfer range from 0.5 to 2.2 F^{-1}. Recently, the Yale group[5] has reported accurate results of inelastic electron scattering from ^{40}Ca which cover the range 0.3–0.6 F^{-1}. A more detailed analysis of the cross section may be made using both our data and those of Yale.

To extract the nuclear parameters, such as spin, parity, and reduced transition probability, from the data of inelastic electron scattering, one must assume some shape for the transition charge density which is characterized by the nuclear model. Results of inelastic electron scattering from various nuclei obtained at Stanford[3,6] were analyzed by means of the Born approximation with the Helm model, which assumes for the transition charge density a Gaussian shape peaked at the nuclear surface. For the same data, Onley, Reynolds, and Wright[7] have demonstrated the use of the distorted-wave calculation using the incompressible and irrotational vibrating-liquid-drop model of Tassie.[8] In this model, the transition charge density is proportional to the first radial derivative of the nuclear surface. The transition charge density of the Tassie model is essentially governed by the same parameters as the ground-state charge distribution. In the case of the Helm model, the parameters may also be taken from the ground-state charge distribution; however, the quality of the Stanford data is insufficient to see the deviations from the strict Helm or from the Tassie model. Recent high-resolution ^{60}Ni(e,e') experiments in the momentum transfer range $0.6 \sim 1.7$ F^{-1} by Torizuka *et al*.[9] have shown that the parameters of the Helm model must be changed to fit the data obtained. Curtis *et al*.[10] have also shown by analyzing both their data and those of Barreau and Bellicard[11] that the Tassie-model predictions could not account for the experimental data of the Sn isotopes.

Quite different transition charge densities based on a shell-model picture, have also been given by Gillet and Melkanoff[12] using the wave functions of

the one-particle—one-hole model calculated by the random-phase approximation (RPA). The RPA theory has successfully described the collective nature of the low-lying states of the doubly-closed-shell nuclei. We have compared our form factors for the 3⁻ and 5⁻ states not only with Tassie's macroscopic nuclear model, but also with the microscopic one-particle—one-hole model.[13,14] We have found that the form factors calculated with the Tassie model do not give adequate fits to the data and also found some discrepancies between the predictions of the particle-hole model and the experimental data.

A value of the reduced transition probability has been extracted by a χ^2 fitting procedure using the transition charge density of a surface-peaked type modified from the Tassie model, and another value of $B(EL)$ has also been extracted by the same procedure assuming a shell-model-type transition charge density similar to that of Gillet and Melkanoff.[12] Then, we have compared the values of $B(EL)$ obtained by assuming the quite different types of the transition charge densities. The actual shapes for the transition charge densities obtained from our analysis are also compared with those predicted by the nuclear models mentioned above.

In addition, the excitations of the dipole states of $T = 0$ and the giant resonance are compared, respectively, with the theoretical results of Fujii and Gillet et al.

II. EXPERIMENTAL METHOD

The output of the Tohoku 300-MeV electron linear accelerator is deflected through 90° to lead into the experimental room, using a pair of bending magnets (M) and a quadrupole magnet (Q) consisting of an M-Q-M system. The quality of the beam was also improved with this magnet system and was designed to be a nondispersive-achromatic-beam transport system. The energy-defining slits placed just behind the quadrupole magnet were set at a momentum width $\Delta p/p_0$ of 0.05% during the present experiment.

The analyzed beam is refocused to a diameter of 3 mm at the target position using a pair of quadrupole magnets. In addition to these magnets, two pairs of steering coils are placed which adjust the vertical and horizontal positions, respectively. The beam spot at the target position is monitored by a closed-circuit television system, using a BeO screen with appropriate calibration markings. This screen is inserted into the beam by remote control at frequent intervals during the experiment. The main sources of the displacement of the beam spot at the target position come from fluctuations of the currents in the focusing solenoids of the lin-

ear accelerator, steering coils, and quadrupole magnets along the drift tubes. The power supply in these systems are stabilized to constrain displacement of the beam spot within ±0.3 mm of the target position.

After passing through the target, the beam was monitored by a secondary emission monitor which was calibrated against a Faraday cup. The beam pipe leading from the analyzing system is connected to the target chamber, using an accelerator guide without rf power supply to protect the accelerator, operating usually at 10^{-8} Torr, from contamination due to hydrocarbon in the target chamber; the guide works as a trap. The target ladder holds five targets, including a BeO screen mentioned above and two graphite plates for the calibration of the cross section and the efficiency of a multichannel detector.

The scattered electrons exit from the target chamber through a wide Mylar window which covers scattering angles from 30 to 165°, and deflected by an $n = \frac{1}{2}$, $\theta = 169.7°$, $r_0 = 100$ cm, double-focusing magnet. This angle was first suggested by Ikegami[15] and Sakai.[16] The magnetic field of the spectrometer was monitored by a rotating-coil fluxmeter.

The electrons are detected with a 33-channel detector ladder lying in the focal plane of the spectrometer. Each channel consists of three lithium-drifted silicon detectors $(2 \times 1 \times 10$ mm) which are operated as a counter telescope. To reduce the background rate for counting electrons, a coincidence was required among three detectors. However, fast coincidence circuits were not used because a solid-state detector, unlike a plastic scintillator, is insensitive to neutron background. The slow coincidences were handled by a computer system. The energy bin defined by each channel was 0.05%, and the range of energies covered by the 33-channel system was 3.3% wide. In order to overlap settings of a counter system, the locations of the settings can be moved stepwise along the focal plane; each step corresponds to the 0.025% shift in energy.

The relative efficiencies of detectors were calibrated by measuring the electrons scattered from the inelastic continuum region in ^{12}C. However, it might be incorrect to regard the measured spectrum as completely flat. The slope of the continuum was measured by varying settings of the spectrometer-magnet currents corresponding to the continuum region, using the multichannel system as a single detector.

Because of a large amount of data accumulated by a multichannel detector in a short time, the data collection was performed by a computer system, enabling a spectrum of the scattered elec-

trons to be immediately displayed on an oscillo-
scope. The raw data were corrected for effects,
such as counting efficiency and counting rate, and
then were printed out and also punched on a tape
for input to the next program. After a run, the
subtraction of the radiative effects was made using
this tape as input, and a spectrum representing
the radiation-corrected data was printed and also
plotted by a curve plotter.

For the present experiment, the energies of the
incident electron were chosen to be 183 and 250

MeV. Varying the scattering angles from 35 to
135°, the corresponding momentum transfer varied
from 0.5 to 2.2 F^{-1}. Some other incident electron
energies were also used in order to separate the
contribution of the transverse excitation, as will
be mentioned later.

An enriched ^{40}Ca target (99.9%, 95.6 mg/cm^2)
supplied from Oak Ridge National Laboratory was
used. To protect from oxidation or other contam-
inations, the ^{40}Ca target was kept in vacuum pump
oil at all times except for measuring.
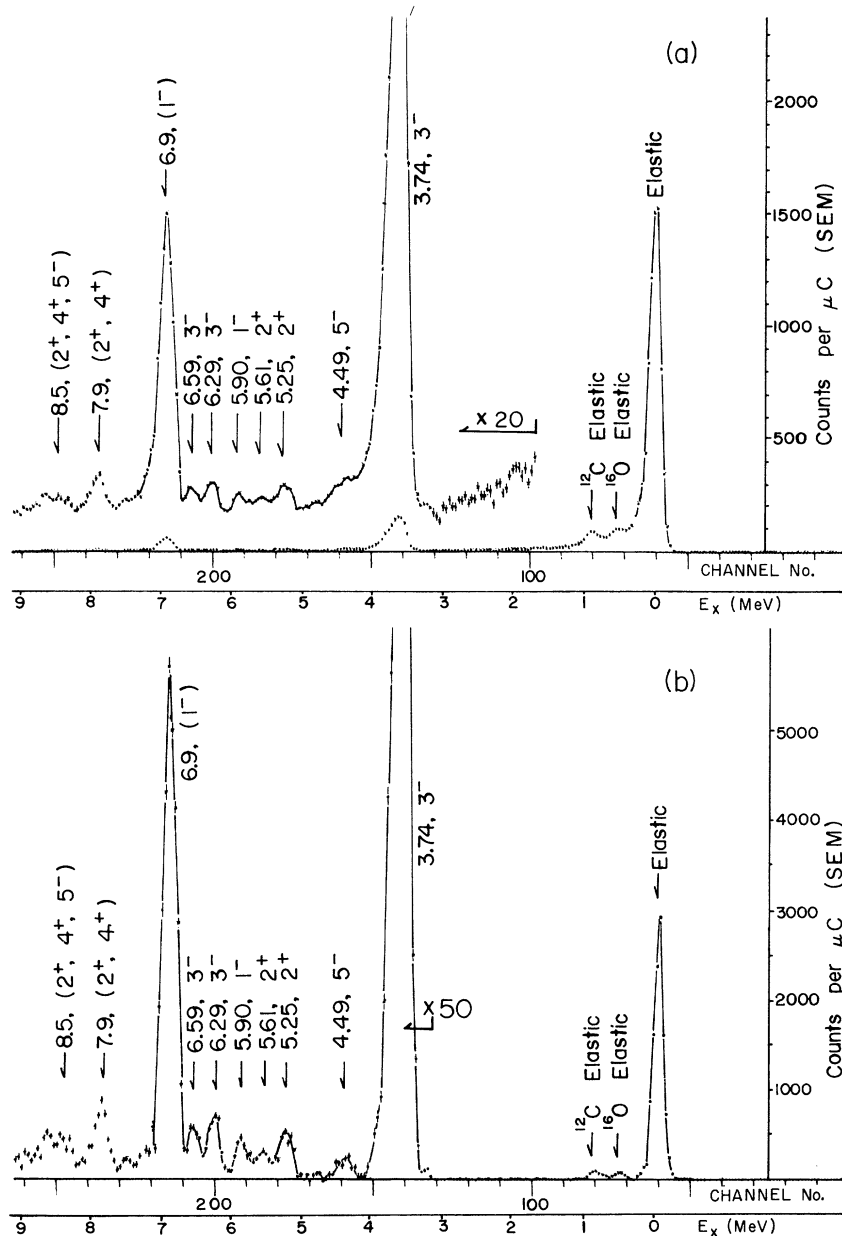
FIG. 1. (a) Spectrum of electrons scattered from ^{40}Ca. The incident energy is 183 MeV and the scattering angle is 55°.
The various peaks may be seen superimposed on the radiative tail due mainly to the elastic scattering peak. (b) The
same spectrum as for (a), except that the radiative corrections have been made.

The absolute cross section of ^{40}Ca was deter-
mined by comparing with the cross section of ^{12}C
and also hydrogen in a CH_2 target. Both proton
and ^{12}C cross sections are known from previous
experiments and theory.[17]

III. RESULTS OF EXPERIMENT

Inelastically scattered electron spectra for ^{40}Ca
are shown in Figs. 1–3. The energies and angles,
183 MeV and 35°, 183 MeV and 55°, and 250 MeV
and 85°, are chosen to obtain values of the momen-
tum transfer favorable for 1^-, 3^-, and 5^- states,
respectively. Both Figs. 1(a) and 2(a) are spectra
with no radiative corrections applied. The usual
radiative corrections were made using the itera-

tive procedure of Crannell.[18] The spectra, after
subtracting the radiative effects by the computer
program, are shown in Figs. 1(b), 2(b), and 3. In
Fig. 3 the spectrum is shown up to an excitation en-
ergy of 25 MeV to display the excitation of the
giant resonance. The full width at half maximum
of the elastic peak was about 0.1%, as was expected
from the experimental conditions. The uncertainty
in determination of the excitation energy was
estimated to be ±100 keV.

The nuclear level scheme for ^{40}Ca obtained by
means of various experimental techniques is
shown in Fig. 4. The levels for which the cross
sections are obtained in the present experiment
are also shown on the right-hand side in the same
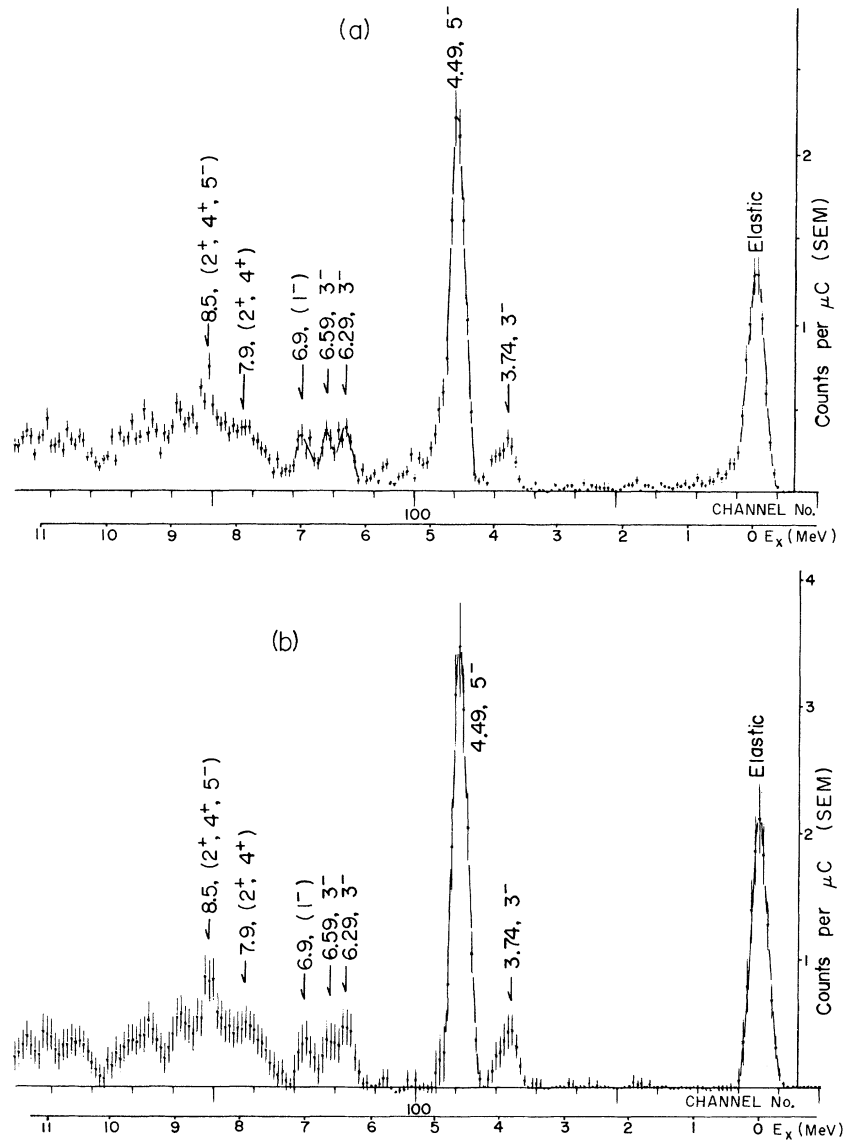
FIG. 2. (a) Spectrum of electrons scattered from ^{40}Ca. The incident energy is 250 MeV and $\theta = 85°$. (b) The same
spectrum as for (a), except that the radiative corrections have been made.
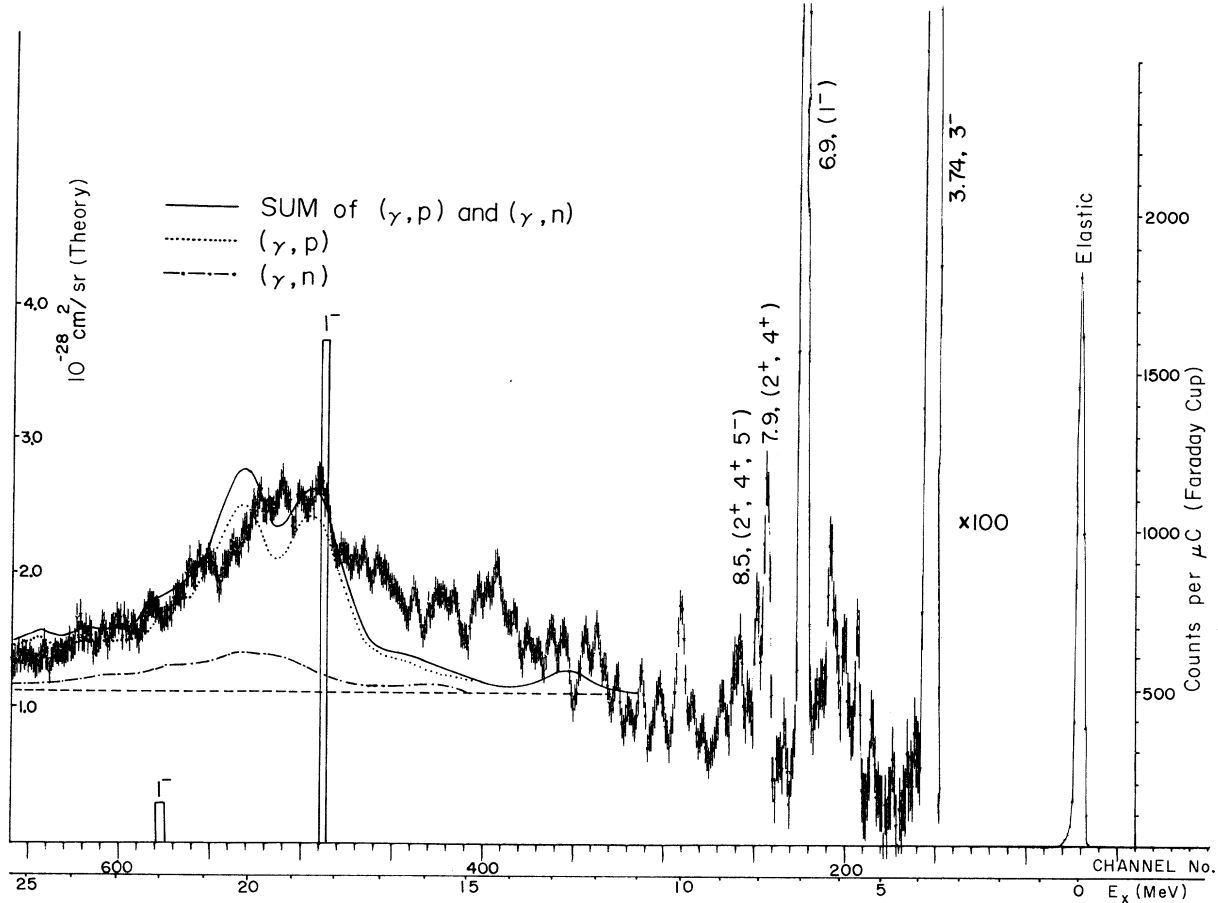
FIG. 3. Spectrum of electrons scattered from ^{40}Ca measured up to the giant-resonance region. The incident energy is 183 MeV and $\theta = 35°$. The radiative corrections have been made. The sum of the cross sections of (γ, p) and (γ, n) reactions are indicated with solid curve on the spectrum.

figure. The values of the cross sections are listed in Tables I and II.

The form factor for inelastic electron scattering is defined by the relation

$$\frac{d\sigma}{d\Omega} = \sigma_{\text{Mott}} |F_{\text{in}}|^2 , \qquad (1)$$

$$\sigma_{\text{Mott}} = (Ze^2/2E_0)^2 \cos^2\tfrac{1}{2}\theta / \sin^4\tfrac{1}{2}\theta , \qquad (2)$$

where $d\sigma/d\Omega$ is the absolute cross section for inelastic scattering and σ_{Mott} is the Mott cross section for elastic scattering through an angle θ of an electron of energy E_0 from a point spinless nucleus without recoil.

In order to compare all the experimental form factors obtained at various energies with a single theoretical curve, the form-factor points were plotted against momentum transfer q. However, q is not uniquely determined as a function of the incident energy and the scattering angle for medium and heavy nuclei. Thus, the cross sections at various energies were normalized to those at 250 MeV with the help of the distorted-wave Born approximation (DWBA) code written by Tuan, Wright, and Onley.[19] The results of the above procedure using the transition charge density, which will be mentioned later, are listed in Table III, where the data of Yale are also included. q is defined by

$$q = (2E_0/\hbar c)\sin\tfrac{1}{2}\theta(1 - \epsilon/E_0)^{1/2} , \qquad (3)$$

where E_0 is 250 MeV and ϵ is the excitation energy for each nuclear level. The form-factor points obtained for values of q between 0.5 and 2.2 F^{-1} for each excitation are shown in Figs. 5, 6, 7, 10, 12, 15, and 16. The data of Yale[5] in the q range 0.3–0.6 F^{-1} are also shown in Figs. 5(a), 6(a), 7, 10(a), 12(a), and 15.

We extract the reduced transition probability and the other nuclear parameters from the experimental data with the DWBA calculation. However, it is also useful to compare the cross section with the plane-wave Born approximation. For the spin-
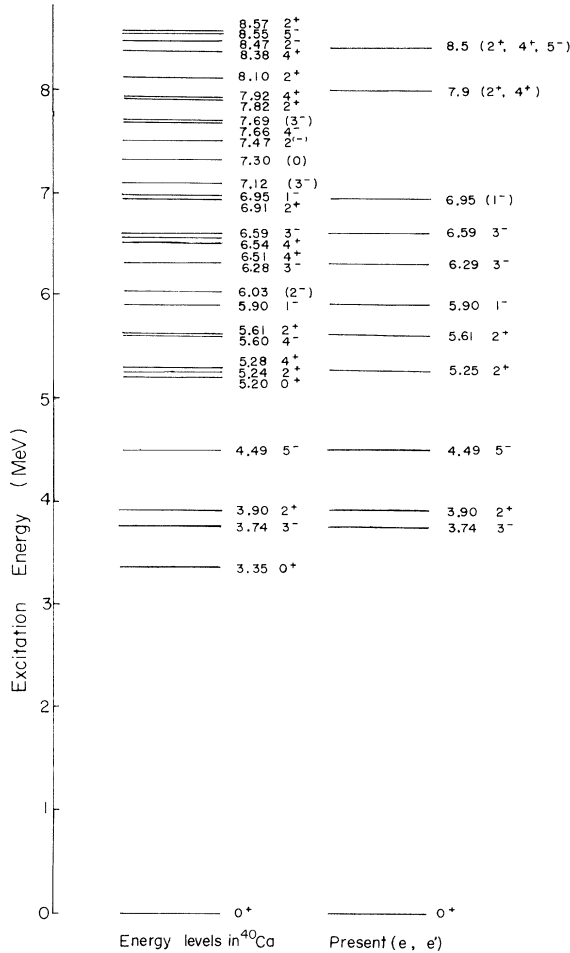
FIG. 4. Nuclear level scheme of ^{40}Ca taken mainly from table of P. M. Endt and C. van der Leun, Nucl. Phys. A105, 1 (1967) (left-hand side), and levels observed by the present electron scattering (right-hand side).

less nucleus, where only one multipole of the electron field contributes to the interaction, the form factor defined by Eq. (1) is expressed by the Born approximation:

$$|F_{in}|^2 = |F_{CL}(q)|^2 + (\tfrac{1}{2} + \tan^2 \tfrac{1}{2}\theta)|F_{EL,ML}(q)|^2 , \quad (4)$$

where $|F_{CL}(q)|$ is the part of the total form factor due to the Coulomb or the longitudinal interaction, and $|F_{EL,ML}(q)|$ is due to the transverse electric part (F_{EL}), or the transverse magnetic part (F_{ML}) of the interaction. These form factors are uniquely determined as functions of the momentum transfer q. When the transverse term contributes to the cross section, the backward-angle enhancement is expected from Eq. (4).

The detection of the transverse form factor may be accomplished by comparing $|F_{in}|^2$ measured at forward and backward angles, using incident energies adjusted to give the same momentum transfer. Such procedures were carried out for the 6.29- (3_2^-), 6.59- (3_3^-), 4.49- (5_1^-), 7.9- $(2^+, 4^+)$, and 8.5-MeV $(2^+, 4^+, 5^-)$ states at the momentum transfer corresponding to 1.6 F^{-1}. The values of $|F_{in}|^2$ obtained for these states are seen in Figs. 5, 6, 10, 12, and 16 as close-lying points either near $q = 1.6$ F^{-1} or 1.8 F^{-1}, or both. We found the contribution of the transverse component to be negligible, within the experimental error, for these data.

IV. COMPARISON WITH NUCLEAR MODELS

For the 3.74- (3_1^-), 4.49- (5_1^-), 6.29- (3_2^-), and 6.59-MeV (3_3^-) states, comparison is made between the experimental data and form factors calculated both with Tassie's vibrational model and with the particle-hole model presented by Gillet and Sanderson.[14] The dipole excitations of the 5.90- (1^-) and

TABLE I. Cross sections for the odd-parity states in ^{40}Ca at the incident energy of 183 MeV. $d\sigma/d\Omega$ are given in units of cm^2/sr with the power of 10 indicated in parenthesis. Errors are expressed as percentage.

E_x θ (deg)	3.74 MeV, 3^- $d\sigma/d\Omega$　error	4.49 MeV, 5^- $d\sigma/d\Omega$　error	5.90 MeV, 1^- $d\sigma/d\Omega$　error	6.29 MeV, 3^- $d\sigma/d\Omega$　error	6.59 MeV, 3^- $d\sigma/d\Omega$　error	6.95 MeV, 1^- $d\sigma/d\Omega$　error
35	$4.36(-30) \pm 7.9$	$1.03(-31) \pm 67.0$	$5.02(-31) \pm 41.1$	$9.91(-31) \pm 24.3$ $8.53(-31) \pm 9.7$	$6.06(-31) \pm 31.8$ $4.68(-31) \pm 39.7$	$4.88(-30) \pm 4.0$
45	$4.21(-30) \pm 10.5$ $4.28(-30) \pm 10.3$	$4.92(-32) \pm 90.0$ $5.41(-32) \pm 72.0$	$2.46(-31) \pm 10.0$ $1.38(-31) \pm 33.3$	$3.22(-31) \pm 11.5$ $4.48(-31) \pm 6.6$	$2.31(-31) \pm 45.7$ $3.20(-31) \pm 34.6$	$2.83(-30) \pm 3.5$ $3.00(-30) \pm 2.5$
55	$2.97(-30) \pm 10.0$ $2.59(-30) \pm 10.9$	$5.99(-32) \pm 25.0$ $6.63(-32) \pm 12.9$	$1.06(-31) \pm 8.1$ $1.30(-31) \pm 10.6$	$1.65(-31) \pm 9.7$ $1.90(-31) \pm 5.6$	$1.44(-31) \pm 10.4$ $1.13(-31) \pm 9.4$	$1.44(-30) \pm 3.7$ $1.38(-30) \pm 3.1$
65	$1.60(-30) \pm 8.3$ $1.56(-30) \pm 8.4$	$5.22(-32) \pm 16.1$ $5.59(-32) \pm 9.4$	$4.79(-32) \pm 8.8$ $4.05(-32) \pm 15.5$	$6.17(-32) \pm 12.0$ $5.95(-32) \pm 6.2$	$4.37(-32) \pm 15.7$ $4.00(-32) \pm 13.0$	$5.69(-31) \pm 2.8$ $5.05(-31) \pm 4.2$
75	$7.72(-31) \pm 7.3$ $6.42(-31) \pm 8.8$	$5.32(-32) \pm 14.3$ $5.48(-32) \pm 6.7$	$1.30(-32) \pm 19.6$ $2.00(-32) \pm 22.5$	$1.95(-32) \pm 21.7$ $1.36(-32) \pm 14.6$	$1.95(-32) \pm 21.7$ $1.70(-32) \pm 15.0$	$2.10(-31) \pm 6.6$ $1.91(-31) \pm 4.5$
85	$3.23(-31) \pm 8.9$	$4.58(-32) \pm 13.3$	$5.30(-33) \pm 48.5$	$4.50(-33) \pm 50.0$	$5.95(-33) \pm 40.5$	$6.80(-32) \pm 9.7$
95	$1.09(-31) \pm 8.7$	$3.31(-32) \pm 15.2$	$1.71(-33) \pm 94.4$	$<2.85(-33)$	$1.90(-33) \pm 85.0$	$1.32(-32) \pm 25.0$
105	$3.47(-32) \pm 9.9$	$2.54(-32) \pm 9.9$				
115	$6.98(-33) \pm 20.1$	$1.49(-32) \pm 12.9$		$1.02(-33) \pm 25.0$	$1.21(-33) \pm 25.0$	$<7.4 \ (-34)$

TABLE II. Cross sections for the odd-parity states in ^{40}Ca at the incident energy of 250 MeV. $d\sigma/d\Omega$ are given in units of cm^2/sr with the power of 10 indicated in parenthesis. Errors are expressed as percentage.

E_x θ (deg)	3.74 MeV, 3$^-$ $d\sigma/d\Omega$ error	4.49 MeV, 5$^-$ $d\sigma/d\Omega$ error	6.29 MeV, 3$^-$ $d\sigma/d\Omega$ error	6.59 MeV, 3$^-$ $d\sigma/d\Omega$ error	6.95 MeV, 1$^-$ $d\sigma/d\Omega$ error
75	$4.96(-32) \pm 24.4$	$6.08(-32) \pm 13.4$	$4.08(-33) \pm 22.2$	$4.84(-33) \pm 31.3$	$4.84(-33) \pm 25.0$
85	$3.44(-33) \pm 20.0$	$3.28(-32) \pm 7.1$	$3.18(-33) \pm 8.1$	$3.44(-33) \pm 10.0$	$3.35(-33) \pm 7.7$
95	$9.66(-34) \pm 31.6$	$1.10(-32) \pm 7.8$			
105	$1.23(-33) \pm 12.5$	$4.67(-33) \pm 6.6$	$1.11(-33) \pm 15.0$	$6.46(-34) \pm 28.6$	$1.44(-33) \pm 12.8$
125	$3.16(-34) \pm 32.1$	$3.50(-34) \pm 22.6$	$8.37(-35) \pm 64.9$	$6.11(-35) \pm 72.2$	$1.58(-34) \pm 50.0$
135 [a]	$7.47(-35) \pm 22.8$	$2.41(-33) \pm 17.9$			

[a] Incident energy is 198 MeV.

6.95-MeV (1$^-$) states are compared with the form factor calculated by Fujii.[20] The data of the giant resonance are also compared with Gillet and Sanderson's model.[14]

A. Tassie Model

A distorted-wave analysis (DWBA) of the form factor for inelastic electron scattering has been developed by a Duke University group, and the analysis of the present experimental data was carried out with the help of the code DUELS of Tuan, Wright, and Onley[19] as mentioned before. This code requires inputs of both the ground-state charge distribution and the transition charge density.

One model of the transition charge density is obtained by Tassie[8] from the incompressible and ir-

TABLE III. Form factors for the 3$^-$ and 5$^-$ states of ^{40}Ca for the incident energy of 250 MeV. The cross sections at various energies were normalized to those at 250 MeV with the help of the DWBA calculation. Errors are expressed as percentage.

θ (deg)	3.74 MeV, 3_1^- q (F^{-1})	$10^4 \times |F_{in}|^2$	6.29 MeV, 3_2^- q (F^{-1})	$10^4 \times |F_{in}|^2$	6.59 MeV, 3_3^- q (F^{-1})	$10^4 \times |F_{in}|^2$	4.49 MeV, 5$^-$ q (F^{-1})	$10^4 \times |F_{in}|^2$
				$E_0 = 60.3$ MeV [a]				
90	0.440	2.22 ± 6.0						
110	0.506	4.50 ± 2.0						
130	0.555	6.66 ± 2.0						
150	0.596	8.65 ± 6.0						
				$E_0 = 183$ MeV				
35	0.552	6.34 ± 7.9	0.549	1.44 ± 24.3 1.24 ± 9.7	0.549	0.88 ± 31.8 0.68 ± 39.7	0.551	0.15 ± 67.0
45	0.702	17.1 ± 10.5 17.4 ± 10.3	0.698	1.31 ± 11.5 1.82 ± 6.6	0.698	0.94 ± 45.7 1.30 ± 34.6	0.701	0.20 ± 90.0 0.22 ± 72.0
55	0.847	27.8 ± 10.0 24.2 ± 10.9	0.842	1.55 ± 9.7 1.78 ± 5.6	0.842	1.35 ± 10.4 1.06 ± 9.4	0.852	0.56 ± 25.0 0.62 ± 12.9
65	0.985	30.3 ± 8.3 29.2 ± 8.4	0.987	1.17 ± 12.0 1.13 ± 6.2	0.979	0.83 ± 15.7 0.76 ± 13.0	0.993	0.99 ± 16.1 1.06 ± 9.4
75	1.125	26.3 ± 7.3 22.7 ± 8.8	1.121	0.69 ± 21.7 0.48 ± 14.6	1.119	0.69 ± 21.7 0.60 ± 15.0	1.130	1.88 ± 14.3 1.94 ± 6.7
85	1.268	20.1 ± 8.9	1.242	0.28 ± 50.0	1.235	0.37 ± 40.5	1.245	2.85 ± 13.3
95	1.372	11.5 ± 8.7	1.360	<0.30	1.350	0.20 ± 85.0	1.353	3.48 ± 15.2
105	1.480	6.02 ± 9.9					1.455	4.41 ± 9.9
115	1.570	1.99 ± 20.1	1.570	0.35 ± 25.0	1.560	0.34 ± 25.0	1.568	4.26 ± 12.9
				$E_0 = 250$ MeV				
75	1.531	3.28 ± 24.4	1.523	0.27 ± 22.2	1.523	0.32 ± 31.3	1.528	4.02 ± 13.4
85	1.699	0.40 ± 20.0	1.690	0.37 ± 8.1	1.689	0.40 ± 10.0	1.696	3.82 ± 7.1
95	1.854	0.19 ± 31.6					1.851	2.17 ± 7.8
105	1.995	0.40 ± 12.5	1.985	0.36 ± 15.0	1.984	0.21 ± 28.6	1.992	1.52 ± 6.6
125	2.231	0.22 ± 32.1	2.219	0.074 ± 64.9	2.218	0.054 ± 72.2	2.227	0.31 ± 22.6
135 [b]	1.845	0.07 ± 22.8					1.841	2.29 ± 17.9

[a] Yale data.   [b] Incident energy is 198 MeV.
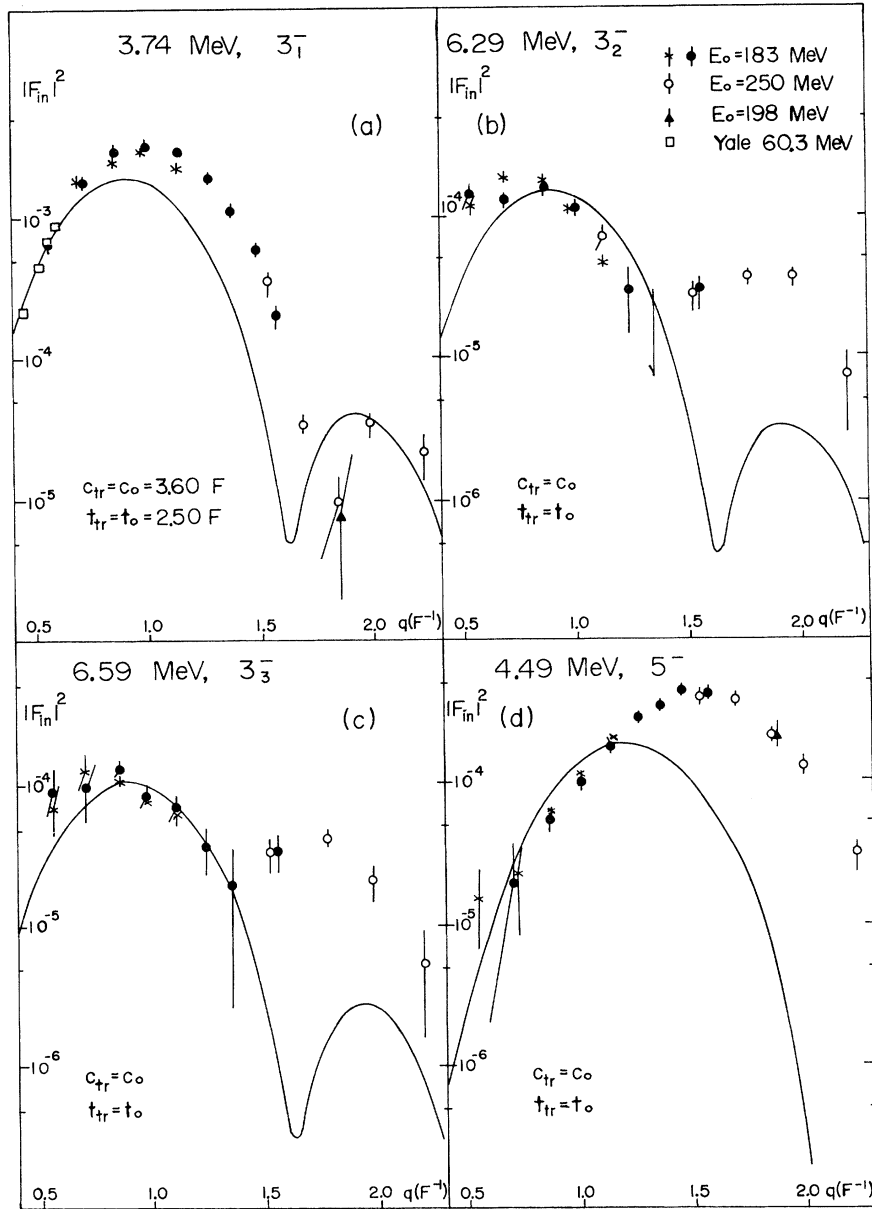
FIG. 5. The experimental $|F_{in}|^2$ for the 3.74- (3_1^-), 6.29- (3_2^-), 6.59- (3_3^-), and 4.49-MeV (5_1^-) states which are defined as $(d\sigma/d\Omega)/\sigma_{Mott}$ are plotted against momentum transfer q. The curves are theoretical cross sections calculated by DWBA code using the transition charge densities of the strict Tassie model.

rotational vibrating-liquid drop:

$$\rho_{tr}(r) = N r^{L-1} \frac{d\rho}{dr} ,\qquad (5)$$

where N is a normalizing factor, L means the multipole order, and ρ is a ground-state charge distribution. The ground-state charge distribution was assumed to be of the Fermi type:

$$\rho(r) = \rho_0 \left[1 + \exp\left(\frac{r-c}{t/4.4}\right) \right]^{-1} ,\qquad (6)$$

where ρ_0 is a normalization charge density, c is the half-density radius, and t is the skin thickness measured between the 10 and 90% points of the charge distribution. The parameters of the ground-state charge distribution can be obtained from an elastic electron scattering experiment. These kinds of measurements were carried out at Stanford and Yale. The values obtained were $c_0 = 3.60$ F and $t_0 = 2.50$ F at Stanford[21] and $c_0 = 3.510$ F for the fixed value of $t_0 = 2.475$ F at Yale.[5]

FIG. 6. The same data as for Fig. 5. The experimental $|F_{in}|^2$ are compared with the theoretical form factors calculated with Gillet-Sanderson wave functions.
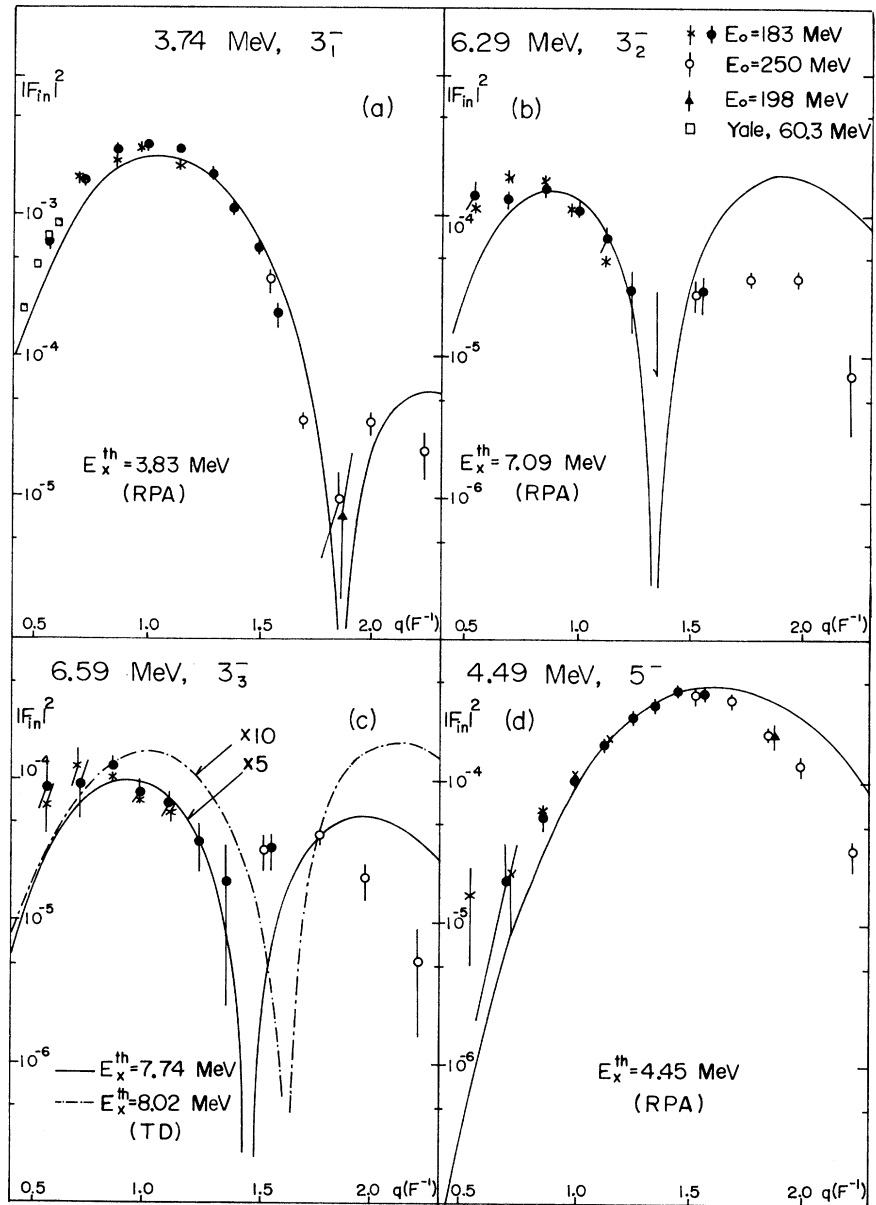
The theoretical form factors for $E3$ and $E5$ excitations were calculated by the use of the DWBA code with the values of the Stanford result. The DWBA curves of the Tassie model for these excitations are compared with the experimental data of the 3.74- (3_1^-), 6.29- (3_2^-), 6.59- (3_3^-), and 4.49-MeV (5_1^-) states, as shown in Fig. 5. The solid curves of the Tassie model do not represent adequate fits to the data of the 3.74- (3_1^-) and 4.49-MeV (5_1^-) states. It may also be seen that the Tassie model does not describe the relative amplitude of the second diffraction maxima of the data of the 6.29-MeV (3_2^-) and 6.59-MeV (3_3^-) states.

B. Particle-Hole Model

Gillet and Sanderson have carried out for ^{40}Ca calculations of the one-particle–one-hole model using both the Tamm Dankoff approximation (TDA) and the RPA. The first result of their calculations were published in 1964[13] and revised in 1967[14] using more-accurate single-particle energies. Using the former, Jolly[22] has calculated the cross sections of the electroexcitations of the odd-parity states of ^{40}Ca and then compared them with the data of Blum, Barreau, and Bellicard.[4] We have calculated the Coulomb form factors using the latter
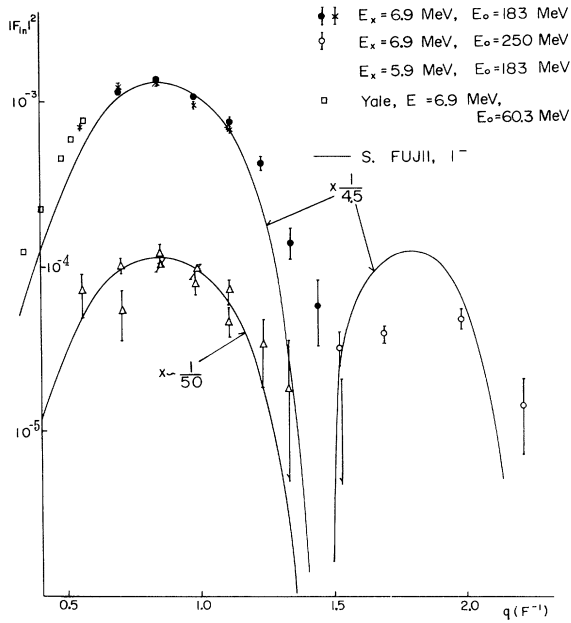
FIG. 7. The experimental $|F_{in}|^2$ for the 5.9-MeV (1^-) and 6.9-MeV states. The solid curves are calculated by Fujii assuming ρ_{tr} which has the form corresponding to the product of monopole and dipole generators.

by means of the Born approximation. The corrections for the finite size of the proton[23,24] and a c.m. motion[23] were introduced into the form factor.

The theoretical form factors for the lowest 3^- state at 3.83 MeV calculated by the use of the RPA is presented in Fig. 6(a). It may be seen that the absolute value of the theoretical curve is in striking agreement with the experimental data of the 3.74-MeV (3_1^-) state.

The theoretical form factors for the 3_2^- and 3_3^- states predicted at 7.09 and 7.74 MeV are compared, respectively, with the 6.29-MeV (3_2^-) and 6.59-MeV (3_3^-) states as shown in Figs. 6(b) and 6(c). The curves for these 3_2^- and 3_3^- states are multiplied by factors of 3 and 5, respectively. The form factor for the predicted 3_4^- state at 8.02 MeV is also shown in Fig. 6(c). Although the absolute values of these form factors are several times lower than the experimental data, it may be seen that the relative amplitudes of the second diffraction maxima of these theoretical curves resemble the q behavior observed rather than the prediction of the Tassie model mentioned in the previous section.

The form factor for the lowest 5^- state at 4.45 MeV calculated by the use of the RPA is compared with the data of the 4.49-MeV (5_1^-) state in Fig. 6(d). Very good agreement for the absolute value may be seen in the lowest 5^- case. However, considering a slight discrepancy of the shape of the theoretical curve with the data, the value of the os-
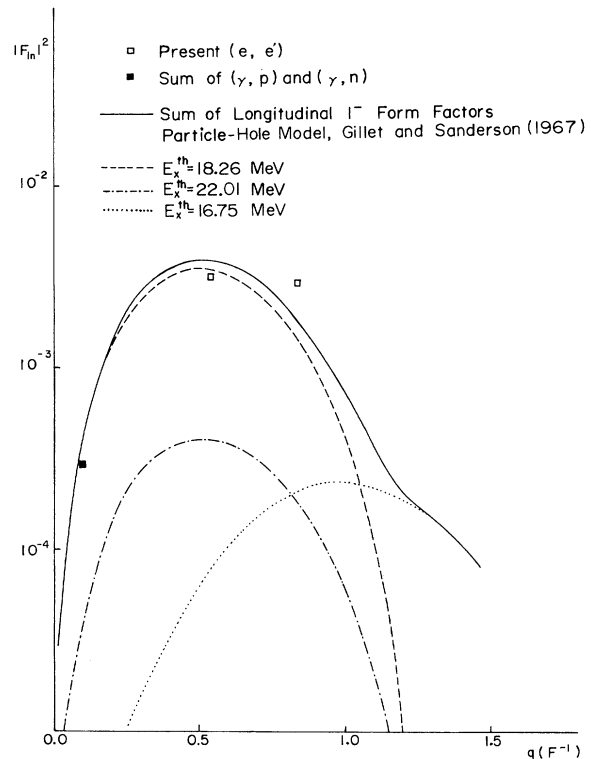
FIG. 8. The experimental form factors of the giant resonance. The data are compared with sum of the theoretical form factors of dipole states calculated with the wave function of Gillet *et al.*

cillator length parameter chosen may not be adequate.

In addition, the predicted second 5^- state at 8.06 MeV is compared with the data of 8.5-MeV excitation as shown in Fig. 16.

C. Fujii Model

It has been reported from the various measurements that there may be 1^-, 2^+, and 3^- states near 6.95 MeV. The (α, α') angular distribution for these states measured by Lippincott and Bernstein[25] is that for a 1^- state and a somewhat weaker positive-parity state. They have also measured the same angular distribution for the known 1^- state at 5.90 MeV. Recently, Metzger,[26] from the resonance-fluorescence experiment, and Kossler,[27] from $^{40}Ca(\alpha, \alpha'\gamma)$ experiment, have confirmed the 1^- state at 6.95 MeV.

However, as may be seen in Fig. 7, the q behavior of the form factor for both of these states is similar to that of an $E3$ transition, apparently inconsistent with the above assignments. In self-conjugate nuclei, such as ^{12}C and ^{16}O, Torizuka *et al.*[28] have found that the q dependence of $E1$ transition with $\Delta T = 0$ in $T_z = 0$ nuclei may show
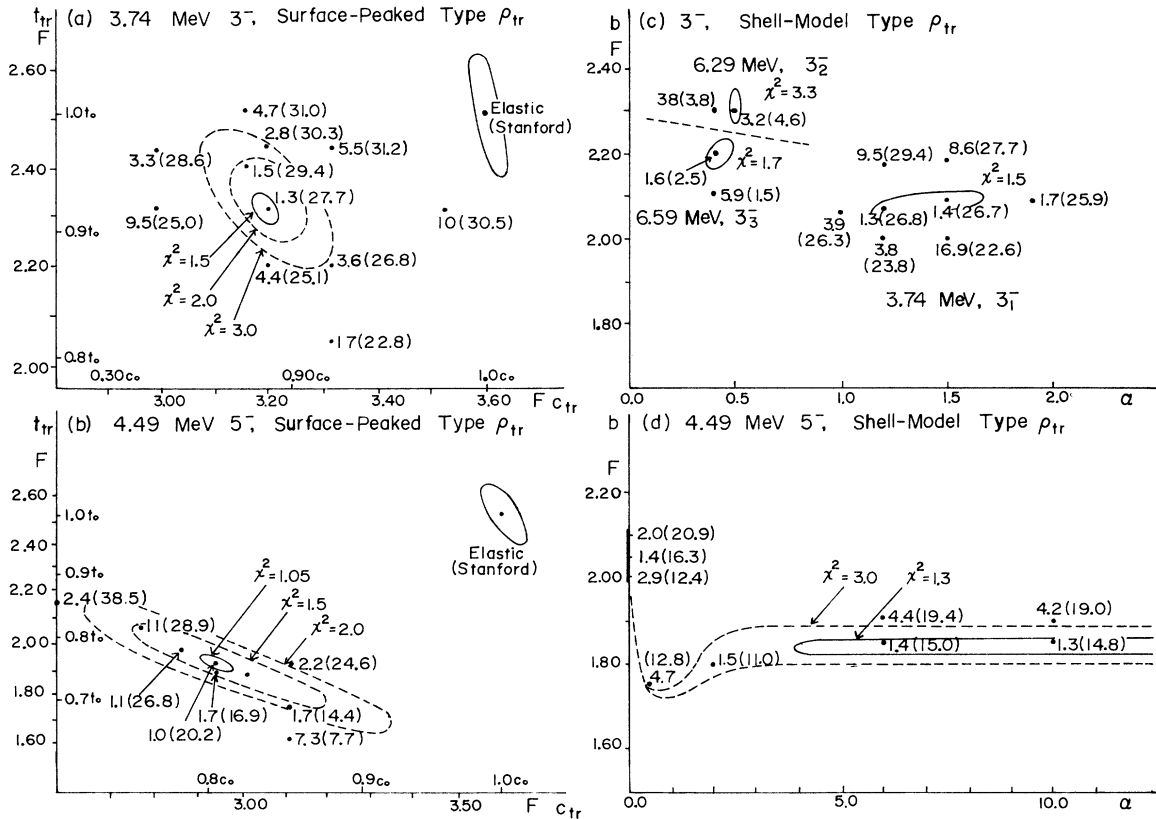
FIG. 9. The results of χ^2 fitting for the 3^- and 5^- states using the transition charge densities of the Tassie type and the particle-hole model type. χ^2 values are plotted against either pair of (c,t) or of (α, b). The $B(EL)$ values are also shown in the parentheses.

that of $E3$-like behavior. According to Fujii's interpretation,[29] this condition is expressed as $\int_0^\infty \rho_{tr} r^3 dr = 0$, which shows that ρ_{tr} must have nodes. He further mentioned that a similar restriction is also found in $E0$ transition. Recently, the possibility of a compressible mode of dipole excitations ($\Delta T = 0$) in ^{12}C and ^{16}O was also examined by Onley.[30]

For the electroexcitation of 1^- $T = 0$ state in ^{40}Ca, Fujii[20] has carried out the calculation of the form factor assuming the following ρ_{tr}:

$$\rho_{tr} \propto \frac{d}{dr}\left[\frac{1}{r^2}\frac{d}{dr}(r^3\rho)\right] , \tag{7}$$

where ρ is the ground-state charge density given by Eq. (6). This form corresponds to the product of dipole and monopole generators. The calculated result is shown in Fig. 7. The q dependence of the data is well reproduced by the shape of the theoretical curve for both the 5.90- and 6.95-MeV states. However, the 6.95-MeV state seems to be the candidate for this mode of excitation, though the experimental form factor is smaller than the theoretical value by a factor of 4.5 for this state.

D. Giant Resonance

We have measured the giant resonance of ^{40}Ca at the relatively forward angles of 35 and 55°, using the incident energy of 183 MeV, where the longitudinal term mainly contributes to the cross section. In Fig. 3, the excitation of the giant resonance around 19 MeV can be seen superimposed on a background which may be due to the process of quasielastic scattering. The curve indicated by solid line on the spectrum is the sum of the (γ,p) and (γ,n) cross sections quoted by Schevchenko.[31]

Our spectrum is compared with the predicition of the dipole excitation calculated by ourselves with the wave function of Gillet and Sanderson.[14] The lengths of the lines are proportional to the values of the calculated cross sections which refer to the left-hand scale in Fig. 3. The electric dipole strength of the particle-hole model is mostly concentrated on the predicted 18.26-MeV state which may correspond to the peak observed around 19 MeV. The quasielastic background is not calculated, but an estimation of its contributions is shown by the dashed line in Fig. 3. Then the cross section, with this background subtracted, is compared
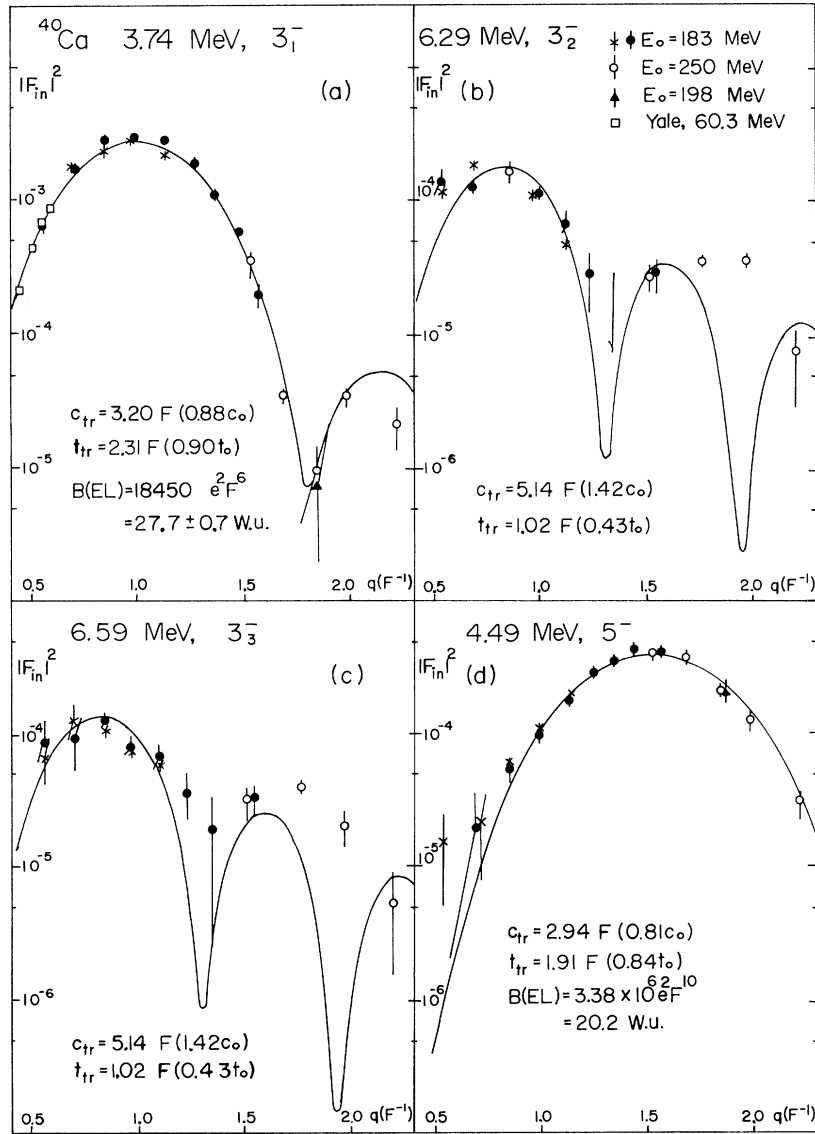
FIG. 10. The same data as for Fig. 5. The curves for the 3_1^- and 5_1^- states are the theoretical cross sections which are achieved by the best fits to the data by χ^2 search with the Tassie type ρ_{tr}. For the 3_2^- or 3_3^- state, it was difficult to achieve a good fit to the second peak of the data within the modification of the Tassie type ρ_{tr}. However, a fairly good theoretical curve obtained with $c_{tr} = 1.42 c_0$ and $t_{tr} = 0.43 t_0$ is shown.

with the theoretical form factor summed over the dipole states at 16.75, 18.26, and 22.01 MeV, as shown in Fig. 8. The form factor at the photon point has been extracted from the sum of the (γ, n) and (γ, p) cross sections.[31] There may be some uncertainties in the subtraction of the background, however, a reasonable agreement between the theoretical and experimental results may be seen. A comparison of our spectrum with those of the (γ, n) and (γ, p) reactions will be further mentioned in Sec. VI.

V. ANALYSIS OF DATA

A. 3.74-, 4.49-, 6.29-, and 6.59-MeV Levels

For these four levels, the experimental form factors were analyzed with the following-type transition charge densities: One is the surface-peaked ρ_{tr} modified from the Tassie model; the other is a shell-model type ρ_{tr} similar to the Gillet-Melkanoff[12] result:

1. Surface-Peaked Type (Tassie Type)

As mentioned in Sec. IV, Tassie's model does
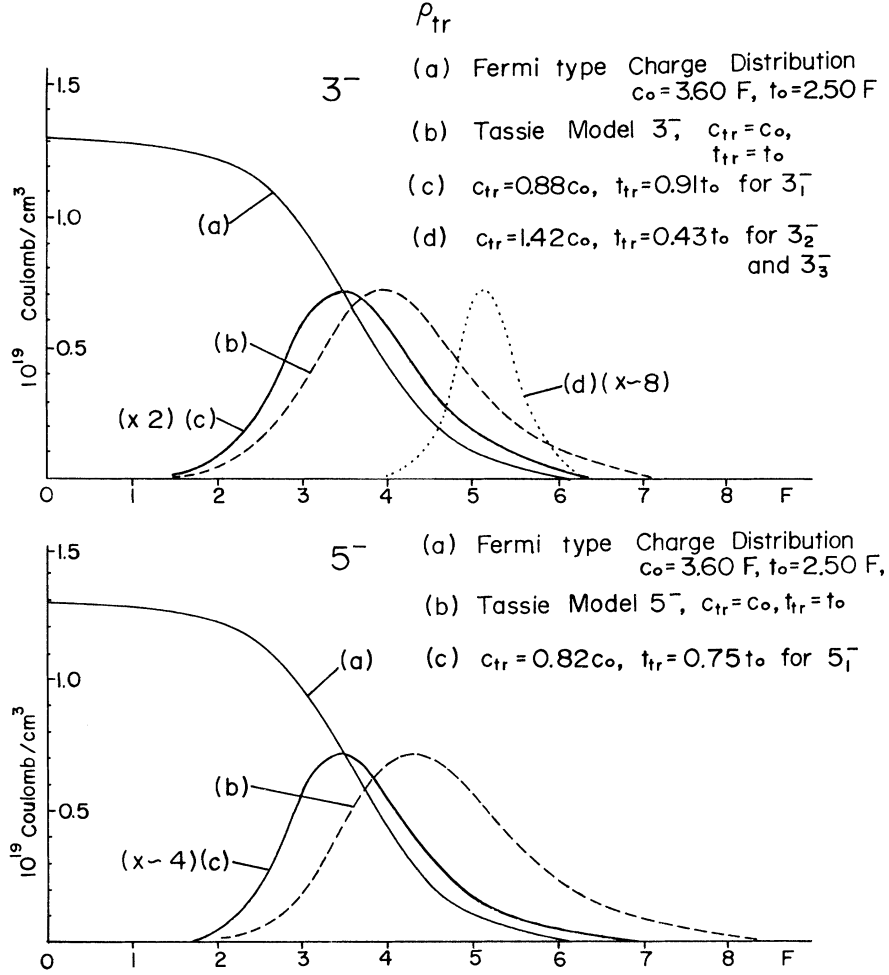
FIG. 11. The comparison between the strict Tassie model ρ_{tr} (dashed curves) and those achieving the best fits to the data by varying the parameters of Tassie type ρ_{tr} for the 3_1^- and 5_1^- states (solid curves). The dotted curve is ρ_{tr} which provides the theoretical curve of the 3_2^- and 3_3^- states in Fig. 10.

not give adequate fits to the data. However, it may be possible to obtain the best fit to the data by varying parameters of the transition charge density from those of the ground-state charge distribution. The DWBA cross sections were fitted to the experimental data by varying the parameters of the transition charge density c_{tr} and t_{tr} until a best fit was achieved, while leaving the ground-state parameters fixed. The values of $B(EL)$ which depend on the parameters can also be extracted in the same calculation, since the calculated DWBA curves are normalized to a unit transition probability, $B(EL) = 1\ e^2\ F^{2L}$. The best-fit values are taken as those which minimize the quantity

$$\chi^2 = \frac{1}{n} \sum_{i=1}^{N} \frac{(\beta |F^{th}|_i^2 - |F^{exp}|_i^2)^2}{(\Delta |F^{exp}|_i^2)^2} \ , \qquad (8)$$

where $|F^{th}|_i^2$ is the ith theoretical form factor, $|F^{exp}|_i^2$ is the ith experimental form factor,

$\Delta |F^{exp}|_i^2$ is the error of ith experimental form factor, N is the number of data points, and n is the degree of freedom $(N-2$ in this case). The adjustable parameter β, with respect to which Eq. (8) is minimized, is directly related to the value of $B(EL)$.

The results of these calculations for the data of the 3.74-MeV (3_1^-) state are shown in Fig. 9(a). The values of χ^2 are plotted for each pair of values of c_{tr} and t_{tr}. Also shown are the contours enclosing $\chi^2 < 1.5$, $\chi^2 < 2.0$, and $\chi^2 < 3.0$. The values of $B(EL)$ in Weisskopf single-particle units[32] corresponding to each pair are given in parentheses. Weisskopf units are defined by

$$B(EL)_{W.u.} = [(2L+1)/4\pi][3/(L+3)]^2 R^{2L}\ e^2\ F^{2L} \ , \qquad (9)$$

with $R = 1.20 A^{1/3}$ F. The values $c_{tr} = 0.88 c_0$, $t_{tr} = 0.9 t_0$, and $B(EL) = 27.7$ W.u. are found to provide
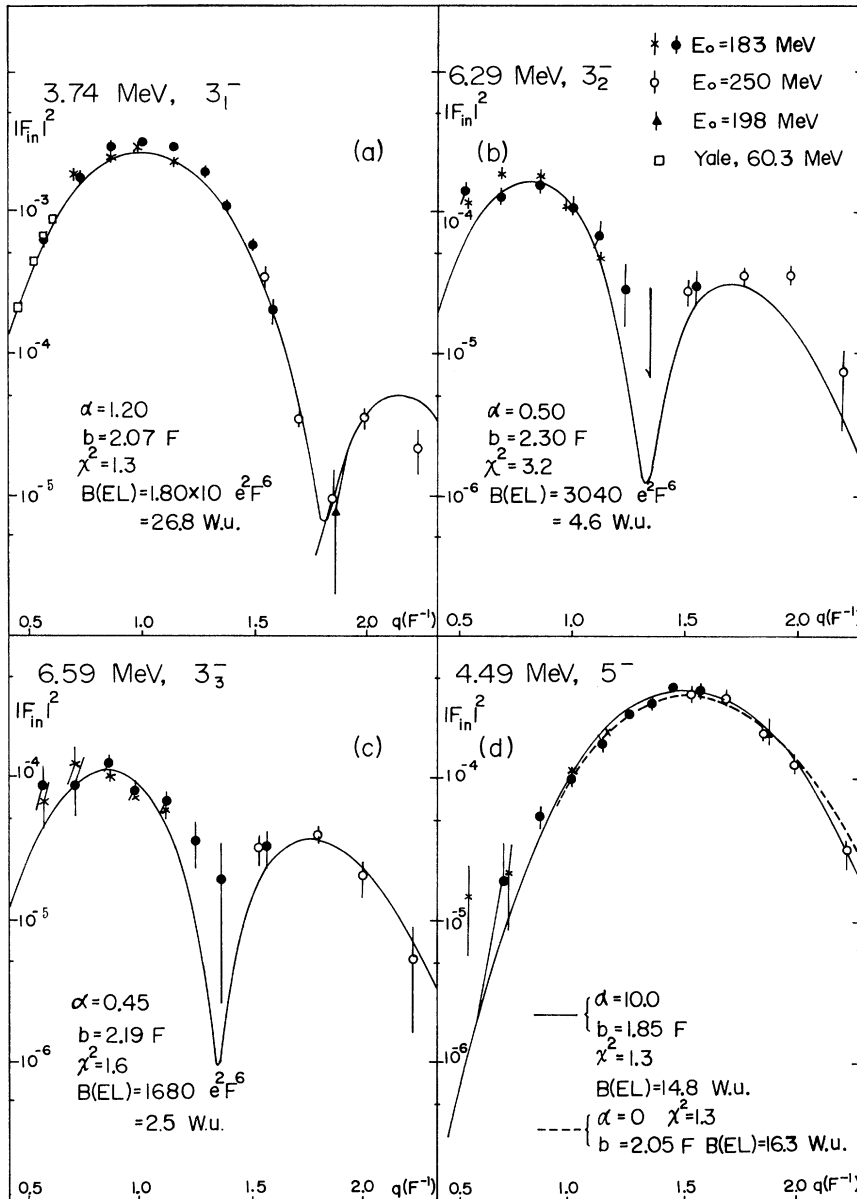
FIG. 12. The same data as for Fig. 5. The curves give the best fits to the data, obtained by varying the parameters of the particle-hole model ρ_{tr}.

the best fit to the data of the 3.74-MeV (3_1^-) state. The theoretical form factor calculated with these parameters is presented in Fig. 10(a).

The same fitting procedure was applied to the data of the 6.29-MeV (3_2^-) and 6.59-MeV (3_3^-) states, however, it was difficult to achieve a good fit to the second diffraction pattern of the data within the modified Tassie model ρ_{tr}. A fairly good theoretical curve with $c_{tr} = 1.42c_0$ and $t_{tr} = 0.43t_0$ is shown for comparison in Figs. 10(b) and 10(c). However, the disagreement between the theoretical form factor and experimental data may be seen in the region of $q > 1.7$ F^{-1}.

The values of χ^2 and $B(EL)$ for 4.49-MeV (5_1^-) state are also shown in Fig. 9(b). The best-fit DWBA curve with $c_{tr} = 0.81c_0$, $t_{tr} = 0.77t_0$, $B(EL)$ = 20.2 W.u. is presented in Fig. 10(d).

The shapes of ρ_{tr} which provide best fits to the data of the lowest 3$^-$ and 5$^-$ states are shown in Fig. 11. These ρ_{tr} (solid curves) are peaked inside the nucleus compared with the predictions of the strict Tassie model (dashed curves). The shape of ρ_{tr} which provides the theoretical curve of the 3_2^- and 3_3^- states in Fig. 10 are also shown in Fig. 11 (dotted curve). This curve is peaked at the extreme edge of the nuclear surface and is
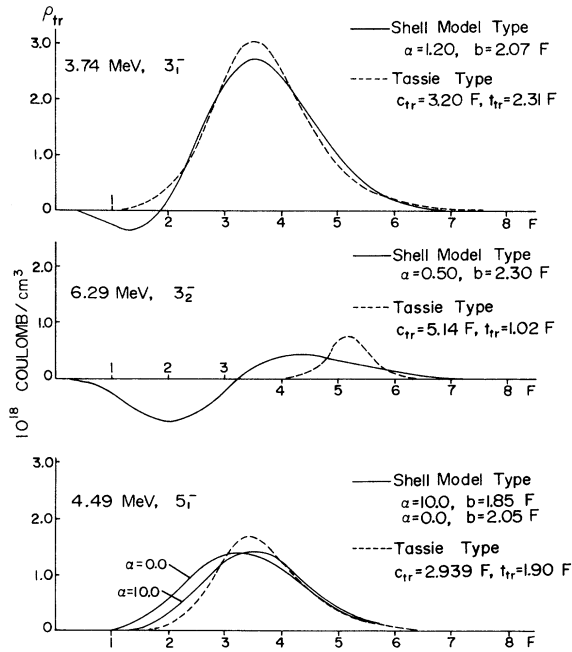
FIG. 13. The shapes of ρ_{tr} which achieved the best fits to the data by varying the parameters of the Tassie and the particle-hole model ρ_{tr} are shown for comparison.

narrower than the Tassie model predicts.

2. Shell-Model Type

The other transition charge densities have been presented by Gillet and Melkanoff[12] for various states of the nuclei ^{12}C, ^{16}O, and ^{40}Ca using the shell-model wave functions. In contrast to the surface-peaked transition charge densities given by the Tassie model, the transition charge densities predicted by Gillet and Melkanoff are peaked well inside the nucleus, and in some case, such as for 3_1^-, $T = 0$ state of ^{40}Ca, the transition charge density does not resemble a Gaussian curve and changes sign as a function of radius.

Although the low-lying collective states are a mixture of many particle-hole configurations, their transition charge densities may be expressed in a simple form, for example, the transition charge densities for 3$^-$ states of ^{40}Ca may be written

$$\rho_{tr}(r) = Ny^3(1 - \alpha y^2)e^{-y^2} \quad , \tag{10}$$

with $y = r/b$, where N is normalizing factor, b may correspond to the oscillator-length parameter, and α determines the position of a node. By choosing proper values of α, b, and N, Eq. (10) completely agrees with the transition charge density for each of the 3$^-$ states of ^{40}Ca given by the Gillet-
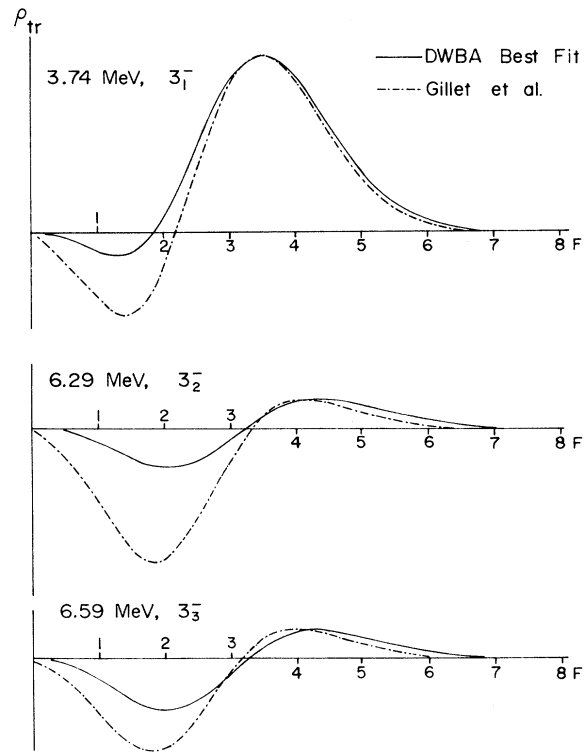
FIG. 14. The comparison of the shell model ρ_{tr} calculated by using Gillet-Sanderson wave functions with the actual ρ_{tr} obtained by fitting procedure. To take into account the finite size of proton, the dash-dotted curves were obtained by folding the proton density into the distribution of the protons in the shell model ρ_{tr}.

Sanderson wave function.

Using Eq. (10), it may also be possible to achieve the best fit to the data by varying α and b in the DWBA calculation. The results of such procedures for the 3.74-MeV (3_1^-), 6.29-MeV (3_2^-), and 6.59-MeV(3_3^-) states are summarized in Fig. 9(c). The values of χ^2 are plotted for each pair of values of α and b. Also shown are the contours enclosing χ^2 < 1.5 for 3_1^-, χ^2 < 3.3 for 3_2^-, and χ^2 < 1.7 for 3_3^- states, respectively. The values of $B(EL)$ in Weisskopf units corresponding to each pair are given in parentheses. The values $\alpha = 1.20$, $b = 2.07$ F, $B(EL) = 26.8$ W.u. provide the best fit to the data of the 3_1^- state. The theoretical form factor calculated with these parameters is shown in Fig. 12(a). The values $\alpha = 0.5$, $b = 2.30$ F, $B(EL) = 4.6$ W.u. and $\alpha = 0.45$, $b = 2.19$ F, $B(EL) = 2.5$ W.u., respectively, are found to provide the best fits to the data of the 3_2^- and 3_3^- states. The DWBA form factors calculated with these parameters are also shown in Figs. 12(b) and 12(c). For all of these states, the agreements between the experimental data and the theoretical curves calculated with the modified
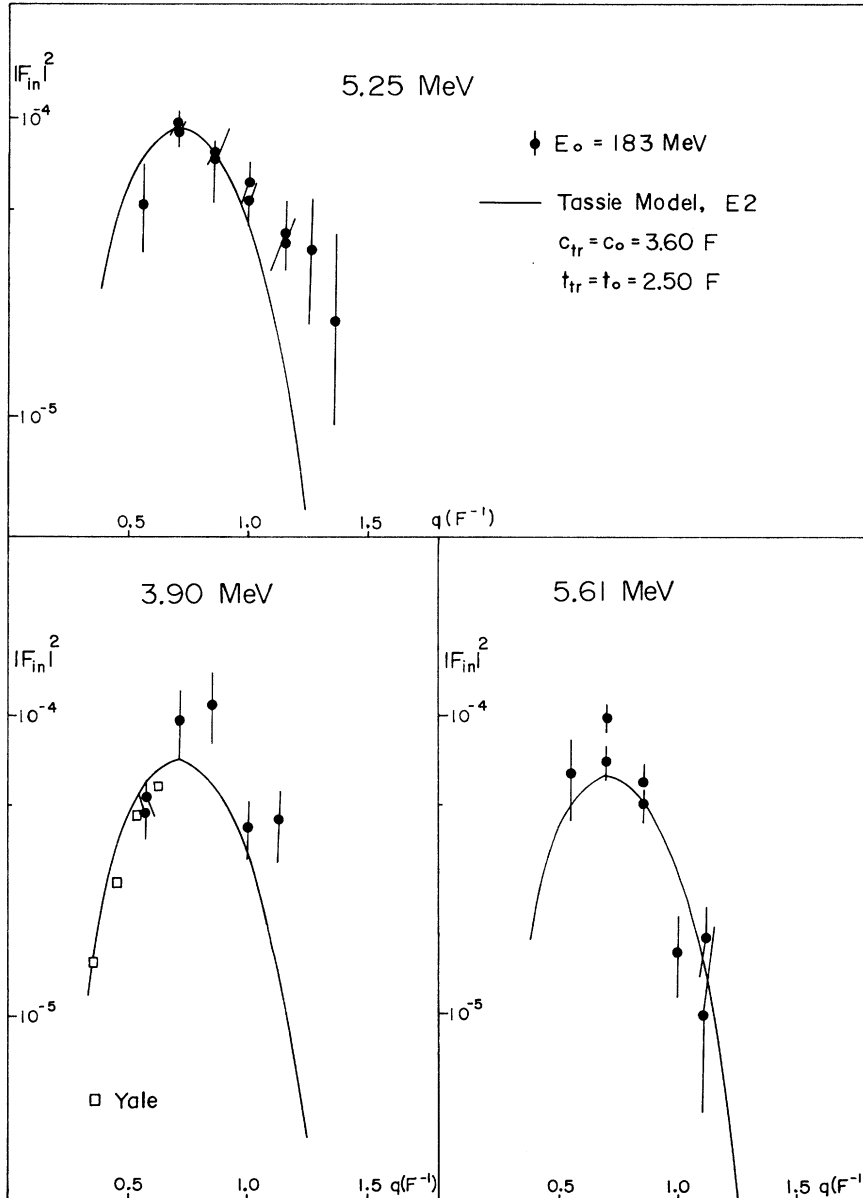
FIG. 15. The experimental $|F_{in}|^2$ for the 3.90-, 5.25-, and 5.61-MeV levels. The curves are calculated by using the strict Tassie model.

shell-model ρ_{tr} are excellent, in contrast to the case of surface-peaked ρ_{tr} mentioned in the previous section. The shapes of the shell-model-type ρ_{tr} which provide the best fits to the data of these states are shown in Fig. 13.

For the 4.49-MeV (5_1^-) state, the shell-model ρ_{tr} may be written as

$$\rho_{tr}(r) = Ny^5(1 - \alpha y^2)e^{-y^2} . \tag{11}$$

With $\alpha = 0$, this form is limited to a $(1f, 1d^{-1})$ configuration corresponding strictly to the result of the particle-hole-model RPA calculation. As the result of a χ^2 search using the form of Eq. (11), we

have found two minimum points which correspond to the values $\alpha = 0$, $b = 2.05$ F, $B(E5) = 16.3$ W.u. and $\alpha = 10$, $b = 1.85$ F, $B(E5) = 14.8$ W.u. as may be seen in Fig. 9(d). The values of the $B(E5)$ obtained from both minimum points agree within the errors. The ρ_{tr} which correspond to these two points are compared in Fig. 13; the similarity of the shapes of ρ_{tr} may be seen. The theoretical form factors corresponding to these ρ_{tr} are shown in Fig. 12(d) with the solid and dotted curves, respectively.

The Tassie-type ρ_{tr} which have indicated in Fig. 11 are also shown for comparison in Fig. 13. Although the primary forms are quite different, the actual shapes obtained for ρ_{tr} are quite similar in
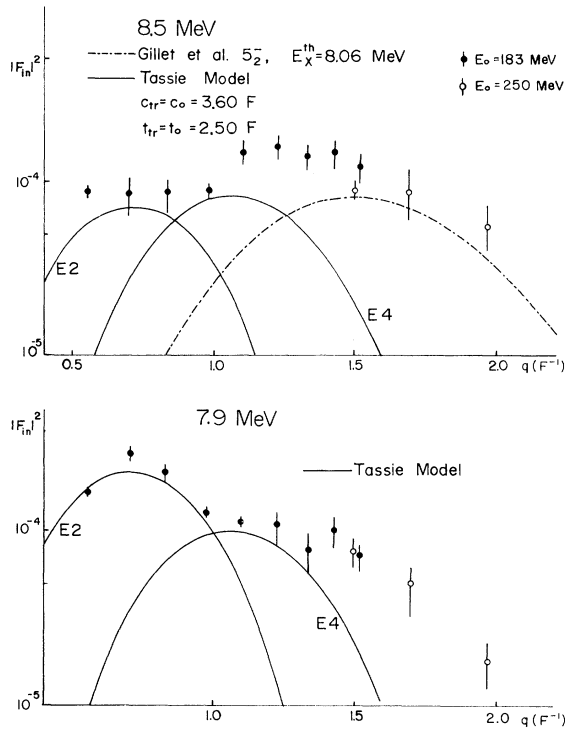
FIG. 16. The experimental $|F_{in}|^2$ for the 7.9- and 8.5-MeV levels. The curves are calculated by Tassie model, except for $E5$ excitation which is calculated by the wave function of Gillet *et al*.

the case of the lowest 3⁻ and 5⁻ states. However, ρ_{tr} for the 3_2^- and 3_3^- states do not overlap between models employed. In Fig. 14 the shell-model ρ_{tr} calculated with Gillet-Sanderson wave functions are compared with the best-fit shell-model-type ρ_{tr}. To take into account the finite size of proton, the presented ρ_{tr} (dash-dotted curves) were smeared by folding the proton density into the distribution of the protons[24] in the shell-model ρ_{tr}.

As may be seen, the actual shapes obtained for ρ_{tr} are quite similar to the theoretical ones.

B. 3.90-, 5.25-, 5.61-, 7.9-, and 8.5-MeV Levels

These levels are weakly excited, or composed of close-lying states, and consequently the errors in the data are not as small as in the previous example. Therefore, it seemed to be meaningless to analyze the data with varying parameters as performed in the previous sections. Thus, the data were analyzed within the limits of the Tassie model.

The form factors of the 3.90-, 5.25-, and 5.61-MeV levels are compared with those of the $E2$ transition, as shown in Fig. 15. The q behavior of the form factors for the 7.9- and 8.5-MeV levels are not simple, as may be seen in Fig. 16. For the 7.9-MeV level, the form factors are compared with the theoretical curves of the $E2$ and $E4$ transitions. The 8.5-MeV level is a complex which may consist of 2⁺, 4⁺, and 5⁻ states, as seen in Fig. 16. The $B(EL)$ values of these states are obtained by hand-fitting analysis using the curves calculated with Tassie-type ρ_{tr}. The values are shown in Table IV. The size of the errors could not be estimated from the present analysis.

VI. DISCUSSION AND COMPARISON

The values of the reduced transition probabilities and parameters of the transition charge densities of the 3⁻ and 5⁻ states obtained from the present experiment are listed in Table V. The $B(EL)$ values, such as for the 3_1^- and 5_1^- states obtained with the different models, are in satisfactory agreement. Therefore, when the $B(EL)$ value is extracted from a fitting procedure which achieves the best fit to the data, the value of $B(EL)$ may not de-

TABLE IV. $B(EL)$ values in Weisskopf units extracted from present (e,e') and other experiments.

E_x (MeV)	J^π	Present Tassie type	Shell-model type	Yale (e,e') (Ref. 5)	Orsay (e,e') (Ref. 4)	MIT (α,α') (Refs. 25, 35)
3.74	3⁻	27.7 ± 1.0	26.8 ± 1.0	31.7 ± 4	15.0	23.6 ± 3.5
3.90	2⁺	3.0 [a]		2.0 ± 0.2	3.6	2.9 ± 0.5
4.49	5⁻	20.2 ± $\frac{9}{5}$	16.3 ± 4.5		12.3	17.7 ± 2.7
5.25	2⁺	0.4 [a]				
5.61	2⁺	0.4 [a]				0.7 ± 0.2
5.90	1⁻					
6.29	3⁻		4.6 ± 0.4			6.6 ± 1.0
6.59	3⁻		2.5 ± 0.2			3.8 ± 0.6
6.95	1⁻					
7.9	2⁺	1.3 [a]				1.8 ± 0.4
7.9	(4⁺)	5 [a]				5.6 ± 0.8
8.5	2⁺	0.4 [a]				0.7
8.5	(5⁻)	7.0 [a]			6.9	2.1(4⁺)

[a] Error was not estimated.

TABLE V. Reduced transition probabilities for the odd-parity states in ^{40}Ca obtained from the different types of transition charge densities.

E_x (MeV)	J^π	Tassie type		Shell-model type	
		$B(EL)$ $(e^2 F^{2L})$	$B/B_{\text{W.u.}}$	$B(EL)$ $(e^2 F^{2L})$	$B/B_{\text{W.u.}}$
3.74	3_1^-	18450 ± 670	27.7 ± 1.0	18000 ± 670	26.8 ± 1.0
		$c_{\text{tr}} = 3.20$ F	$t_{\text{tr}} = 2.31$ F	$\alpha = 1.20, b = 2.07$ F	
4.49	5^-	$(3.38 \pm {}^{1.52}_{0.85}) \times 10^6$	$20.2 \pm {}^9_5$	$(2.73 \pm 0.75) \times 10^6$	16.3 ± 4.5
		$c_{\text{tr}} = 2.94$ F	$t_{\text{tr}} = 1.91$ F	$\alpha = 0.00, b = 2.05$ F	
6.29	3_2^-			3040 ± 260	4.6 ± 0.4
				$\alpha = 0.50, b = 2.30$ F	
6.59	3_3^-			1680 ± 130	2.5 ± 0.2
				$\alpha = 0.45, b = 2.19$ F	

pend strongly on a particular functional form for the transition charge density. The values of the parameter b, which may be related to the oscillator-length parameter, lie in a relatively small range for both the lowest 3$^-$ and 5$^-$ states and are close to the value of 2.08 F determined by the analysis of elastic electron scattering.[13]

The results of the other ^{40}Ca (e, e') experiments are also shown in Table IV. The $B(EL)$ value of Yale for the 3_1^- state is slightly higher than ours. It may be attributed to the difference of the parameters in ρ_{tr}. The Yale values $c_{\text{tr}} = 1.017 c_0$ and $t_{\text{tr}} = 1.01 t_0$ do not provide fits to our high-q data. Serious disagreements of the $B(EL)$ values of Blum, Barreau, and Bellicard[4] with ours are seen. We infer that discrepancies may lie in the energy resolution of the measurement and the method of analysis employed.

In the case of the 6.95-MeV state, Eisenstein et al.[5] have interpreted it as a complex of 2$^+$ and 3$^-$ states and Blum, Barreau, and Bellicard[4] as a 3$^-$ state. However, we have compared the data of this state with the theoretical curve of $E1$ excitation, as mentioned in Sec. IV C. If the 6.95-MeV level is assumed to be a pure 3$^-$ state, the $B(E3)$ value extracted from our data is about 30 W.u., in-

TABLE VI. Theoretical and experimental reduced transition probabilities for odd-parity states.

E_x (MeV)	J^π	Present	Horie and Yokozawa (Ref. 33)	Gerace and Green (Ref. 34)
3.74	3_1^-	27.3 ± 1.0 [a]	25.0	27.2 (23.0)[b]
6.29	3_2^-	4.6 ± 0.4		1.9 (0.5)
6.59	3_3^-	2.5 ± 0.2		2.7 (3.5)
4.49	5^-	17.7 ± 3.8 [a]	23.4	20.4 (18.0)

[a] Weighted mean of $B(EL)$ from Tassie-type and shell-model-type transition charge density.

[b] $B/B_{\text{W.u.}}$ in parentheses were calculated on a different basis of single-particle energy I (see Ref. 34).

consistent with the shell-model predictions of Horie and Yokozawa,[33] Gillet et al., and Gerace and Green[34] where the octupole strength mostly concentrates on the lowest octupole state. However, it should be noticed that the second dipole state at 6.95 MeV in ^{40}Ca is markedly stronger than the first one at 5.90 MeV, unlike the octupole case mentioned above.

Our $B(EL)$ values are also compared with the isoscalar transition strengths obtained from (α, α') reaction as shown in Table IV. These isoscalar values are calculated by Bernstein[35] assuming the vibrations of a Fermi mass distribution. It may be seen for the highly enhanced states, such as the lowest 3$^-$ and 5$^-$ state, close agreement is obtained between the isoscalar and the electromagnetic transition strengths.

In the giant-resonance region, our spectrum is compared with sum of the (γ, n) and (γ, p) cross sections,[31] as shown in Fig. 3. For the real photon absorption, the value of the momentum transfer is uniquely determined from a single energy transfer, thus the difference between the two values of momentum transfer is very large, however, the general shapes of the spectra in Fig. 3 are quite similar. This suggests that both spectra are dominantly excited by the same mode.

In Table VI our $B(EL)$ values are compared with the theoretical values of Horie and Yokozawa and Gerace and Green. Horie and Yokozawa have limited the calculation, like Gillet and Sanderson, within the one-particle–one-hole model. On the other hand, Gerace and Green extend the usual 1p-1h calculation by adding a 3p-3h state for the odd-parity states. They also include the additional effect of a polarized core for above calculation. Beautiful agreement is obtained between the theoretical and experimental $B(EL)$ values, as seen in Table VI. However, the direct comparison of the theoretical predictions with the experimental cross sections may be a more crucial test for selection among the various approximations.

[1] W. C. Barber, Ann. Rev. Nucl. Sci. 12, 1 (1962).

[2] T. deForest and J. D. Walecka, Advan. Phys. 15, 1 (1966).

[3] R. Helm, Phys. Rev. 104, 1466 (1956).

[4] D. Blum, P. Barreau, and J. Bellicard, Phys. Letters 4, 109 (1963).

[5] R. A. Eisenstein, D. W. Madsen, H. Theissen, L. S. Cardman, and C. K. Bockelman, Phys. Rev. 188, 1815 (1969).

[6] H. Crannell, R. Helm, H. Kendall, J. Oeser, and M. Yearian, Phys. Rev. 123, 923 (1961).

[7] D. S. Onley, J. T. Reynolds, and L. E. Wright, Phys. Rev. 134, B945 (1964).

[8] L. J. Tassie, Australian J. Phys. 9, 407 (1956).

[9] Y. Torizuka, Y. Kojima, M. Oyamada, K. Nakahara, K. Sugiyama, T. Terasawa, K. Itoh, A. Yamaguchi, and M. Kimura, Phys. Rev. 185, 1499 (1969).

[10] T. H. Curtis, R. A. Eisenstein, D. W. Madsen, and C. K. Bockelman, Phys. Rev. 184, 1162 (1969).

[11] P. Barreau and J. Bellicard, Phys. Rev. Letters 19, 1444 (1967).

[12] V. Gillet and M. A. Melkanoff, Phys. Rev. 133, B1190 (1964).

[13] V. Gillet and E. A. Sanderson, Nucl. Phys. 54, 472 (1964).

[14] V. Gillet and E. A. Sanderson, Nucl. Phys. A91, 292 (1967).

[15] H. Ikegami, Rev. Sci. Instr. 29, 943 (1958).

[16] M. Sakai, Nucl. Instr. Methods 8, 61 (1960).

[17] R. Hofstadter, *Nuclear and Nucleon Structure* (W. A. Benjamin, Inc., New York, 1963).

[18] H. Crannell, Phys. Rev. 148, 1107 (1966).

[19] S. T. Tuan, L. E. Wright, and D. S. Onley, Nucl. Instr. Methods 60, 70 (1968).

[20] S. Fujii, private communication.

[21] R. F. Frosch, R. Hofstadter, J. S. McCarthy, G. K. Nöldeke, K. J. Van Oostrum, B. C. Clark, R. Herman, and D. G. Ravenhall, Phys. Rev. 174, 1380 (1968).

[22] H. P. Jolly, Nucl. Phys. 67, 209 (1965).

[23] L. J. Tassie and F. C. Barker, Phys. Rev. 103, 940 (1958).

[24] L. R. B. Elton, *Nuclear Size* (Oxford University Press, London, England, 1961).

[25] E. P. Lippincott and A. M. Bernstein, Phys. Rev. 163, 1170 (1967).

[26] F. R. Metzger, Phys. Rev. 165, 1245 (1968).

[27] W. J. Kossler, Phys. Rev. 165, 1209 (1968).

[28] Y. Torizuka, M. Oyamada, K. Nakahara, K. Sugiyama, Y. Kojima, T. Terasawa, K. Itoh, A. Yamaguchi, and M. Kimura, Phys. Rev. Letters 22, 544 (1969).

[29] S. Fujii, Progr. Theoret. Phys. (Kyoto) 42, 416 (1969).

[30] D. S. Onley, Nucl. Phys. A149, 197 (1970).

[31] Quoted by V. G. Schevchenko, J. Phys. Soc. Japan Suppl. 24, 397 (1968).

[32] K. Adler, A. Bohr, T. Huus, B. Mottelson, and A. Winter, Rev. Mod. Phys. 28, 432 (1956).

[33] H. Horie and T. Yokozawa, Phys. Letters 7, 145 (1963).

[34] W. J. Gerace and A. M. Green, Nucl. Phys. A113, 641 (1968).

[35] A. M. Bernstein, in *Advances in Nuclear Physics*, edited by M. Baranger and E. Vogt (Plenum Press, Inc., New York, 1969), Vol. 3.